

# Modified Fractional Order PID Controller for Load Frequency Control of Four Area Thermal Power System

Ahmed Saba Mohammed <sup>a,1,\*</sup>, Tajudeen Humble Sikiru <sup>b,2</sup>, Ibrahim Bello <sup>c,3</sup>,  
Ahmed Tijani Salawudeen <sup>d,4</sup>, Usman Alhaji Dodo <sup>e,5</sup>

<sup>a, b</sup> Department of Computer Engineering, Ahmadu Bello University Zaria, Nigeria

<sup>c</sup> Dyson Technology, United Kingdom

<sup>d</sup> Department of Electrical and Computer Engineering, University of Jos, Nigeria

<sup>e</sup> Department of Electrical and Computer Engineering, Base University Abuja, Nigeria

<sup>1</sup> [msahmed5050@gmail.com](mailto:msahmed5050@gmail.com); <sup>2</sup> [sikiruhumble02@gmail.com](mailto:sikiruhumble02@gmail.com); <sup>3</sup> [ibrahim.bello@ieee.org](mailto:ibrahim.bello@ieee.org); <sup>4</sup> [elteejayy@gmail.com](mailto:elteejayy@gmail.com);

<sup>5</sup> [usman.dodo@baseuniversity.edu.ng](mailto:usman.dodo@baseuniversity.edu.ng)

\* Corresponding Author

## ARTICLE INFO

## ABSTRACT

### Article history

Received January 20, 2023

Revised March 22, 2023

Accepted March 24, 2023

### Keywords

Load frequency control;

Fractional order PID

controller;

Ant lion optimizer algorithm;

Integral square error

This paper presents the development of a modified Fractional Order Proportional Integral Derivative (FOPID) controller to mitigate frequency deviation in a four-area thermal power system. Change in load demand and noisy power system environment can cause frequency deviation. Reducing high-frequency deviation is very paramount in load frequency control. This is because large frequency deviation can cause the transmission line to be overloaded, which may damage transformers at the transmission level, damage mechanical devices at the generating stations and also damage consumer devices at the distribution level. The conventional PID has been widely used for this problem. However, the parameter values of the various generating units of the power system like generators, turbines and governors keep changing due to numerous on/off switching in the load side. As such, it is essential that the control strategy applied should have a good capability of handling uncertainties in the system parameters and good disturbance rejection. Fractional order PID controller is known to give a higher phase margin resulting in very good disturbance rejection, robustness to high-frequency noise and elimination of steady-state error. A four-area power system was designed, and FOPID was used as the supplementary controller to mitigate frequency deviation. Ant Lion Optimizer (ALO) algorithm was used to optimize the gains of the FOPID controller by minimizing Integral Square Error (ISE) as the objective function. Results obtained outperformed other designed methods available in the literature in terms of reducing frequency deviation, tie-line power deviation and area control error.

This is an open-access article under the [CC-BY-SA](https://creativecommons.org/licenses/by-sa/4.0/) license.



## 1. Introduction

The networks that consist of the generation, transmission and distribution of electrical energy can be referred to as power systems. Power system control can be seen as maintaining a balance between electrical power generation and load demand. The power system has two control loops, namely: primary and secondary control loops [1]. Primary control is the turbine-governor system within the

plant which is used to balance only the reactive power [2][3]. In an interconnected system, the primary control is not enough because of the steady state frequency error due to reactive power balance in the primary control loop [4]-[8]. Since it is required to reduce frequency deviation in all areas of an interconnected power system, another level of power balance called supplementary/secondary control is introduced within a large-scale (multi-area) power system [9]. Power system control can be categorized into two: the first part relates to frequency or active power balance, while the second part is related to voltage regulation or reactive power balance [10][11]. The reactive power plus voltage control is generally known as Automatic Voltage Regulator [12]. The active power plus Load Frequency Control (LFC) is also known as Automatic Load Frequency Control (ALFC) [13]. To maintain stability when there exists variation in transmission line power flow and the active power demand, Automatic Load Frequency Control (ALFC) is required [14].

Amongst the problems of large-scale power systems is the imbalance between generated power and load demand which is due to the changes in parameter values of the various generating units of the power system. These parameter changes are due to numerous on/off switching in the load side [15]-[19]. The process of maintaining the balance between load demand and generated power together with scheduled transmission line power exchange and system losses is referred to as Load Frequency Control (LFC) [20]-[22]. Some conventional LFC uses an integral controller whose dynamic performance is restricted by integral gain and also does not have a good capability of handling uncertainties in the system parameters [29][41]. A high integral gain can impair the performance of a system resulting in an undamped system [42].

Fractional Order Proportional Integral Derivative (FOPID) Controller is expressed by a fractional order differential equation where the fractional part of the integral and derivative can be a positive integer or zero [32][34]. A fractional order PID controller is known to have a very good capability of handling parameter uncertainty. It gives a higher phase margin resulting in very good disturbance rejection, robustness to high-frequency noise and elimination of steady-state error. As such, the control system response can be improved when the integral and derivative of a PID controller are expanded into fractional order [36][39].

The importance of load frequency control in a physical system is to minimize large frequency deviation. Several kinds of research have been conducted in the area of load frequency control with and without nonlinearities. A PID controller based on Linear Matrix Inequality (LMI) for a single and multi-area power system was proposed by [1]. A new PID controller for interconnected power systems via Direct Synthesis (DS) method was investigated [4]. The effects of GDB were investigated by [7] using Redox Flow Batteries (RFB) together with Unified Power Flow Controller (UPFC) to improve the LFC of a multi-source interconnected power system. A controller for LFC of power systems for single and multi-area cases was presented by [33]. Laurent Series was used to obtain the gain of the PID controller by expanding the controller transfer function. A FOPID controller to minimize the deviation in frequency of a single-area power system considering non-reheat, hydro and reheat turbines was investigated in [39][40]. The effects of GRC and GDB nonlinearities on LFC of power systems with reheat, non-reheat and hydro turbines were investigated in [41]-[45], and an anti-windup scheme was added to the designed power system in order to retain the performance and stability of the system.

Artificial Bee Colony algorithm based load frequency controller for an interconnected power system was presented in [7], and Particle Swarm Optimization (PSO) was used to optimize the gains of FOPID controller for LFC of two-area non-reheat thermal power systems in [10]. The effects of GRC were investigated in [13], where the differential evolution algorithm was used to optimize the fractional integral term and integer order Proportional and Derivative gain to minimize frequency deviation in a three-area power system. The effects of non-reheat and reheat turbines in a two-area power system with physical constraints such as GDB, time delay and GRC were investigated by [16], and an integral controller optimized using a genetic algorithm was used to minimize the deviation in frequency. Load frequency control of power systems using FOPID based on the Big Bang Big Crunch (BB-BC) optimization algorithm and IMC scheme had been presented by [21]. An optimized FOPID

and a Tilted Integral Derivative with Filter (TIDF) controller for a two-area multi-source power system were presented by [27]. Parameters of PID, TIDF and FOPID controller were obtained using the Differential Evolution algorithm. A PI controller optimized using the ant lion optimizer algorithm to minimize deviation in frequency of a three-area power system was presented by [35].

In the power system, frequency deviation is to be minimized at all times so as to maintain the balance between the generated power and load demand. This is difficult to attain because of differences in the load demand of each area. Large frequency deviation normally occurs when the differences in load demand and the generated power are high. As such, the performance of the load frequency controller is degraded even for a small load perturbation. These changes in load demand normally occur due to the switching on/off at the load side, thereby making it difficult to minimize frequency deviation even with a robust load frequency controller [45]. Several kinds of research have been conducted on minimizing the frequency deviation of a four-area power system [4]. Yet the system suffers from large frequency deviation and longer settling time due to the changes in load demand of each area. Results obtained show that frequency deviation was mitigated when a robust controller was used as the supplementary control scheme.

In this paper, a Fractional Order Proportional Integral Derivative (FOPID) controller to reduce large frequency deviation in a four-area interconnected power system will be presented. The efficiency of the proposed method will be verified in terms of frequency deviation, tie-line power deviation, area control error and settling time by applying a load disturbance to the system. Results obtained show an improvement in minimizing frequency deviation, area control error of each area and the tie-line power deviation of the connected areas when compared to other design methods available in the literature. Such methods include a Proportional Integral Derivative controller based on Linear Matrix Inequality Singh et al. [1] and Proportional Integral Derivative controller based on the Direct Synthesis approach Anwar & Pan [4].

The rest of the paper is organized as follows. Power system modeling and description will be given in Section 2. The description of the Fractional Order PID controller will be given in Section 3. The methodology and the description of the optimization algorithm will be given in Section 4. Simulations, results and discussions will be given in Section 5. The conclusion and further works will be discussed in Section 6.

## 2. Power System Modeling and Description

Power system configuration for load frequency control will be discussed in this section. A four-area thermal power system has three major components: a governor, a turbine and a generator discussed in [1]. The supplementary/secondary control loop is used to return the frequency to its nominal value [24]. The block diagram of a four-area power system network is shown in Fig. 1.

### 2.1. Turbines

Turbines are devices used for converting energy obtained from water and steam into mechanical energy that can be fed into the generator [34]. There are three types of turbines hydraulic turbines, the non-reheat and reheat turbines. Each of these turbines can be mathematically modeled by a transfer function. Reheat turbines are represented by second-order units, whereas a non-reheat turbine can be modeled by a first-order unit [30][31]. For this paper, a non-reheat and reheat turbine will be considered. The transfer functions of a non-reheat turbine are given in (1)

$$\frac{\Delta P_T(s)}{\Delta P_V(s)} = \frac{1}{1 + sT_T} \quad (1)$$

where  $\Delta P_V(s)$  represents the turbine input,  $\Delta P_T(s)$  is the turbine output and  $T_T$  is the turbine time constant.

The transfer function for the reheat turbine is represented by (2)

$$G_{T-R} = \frac{CT_r s + 1}{(T_r s + 1)(T_t s + 1)} \tag{2}$$

where  $T_r$  is a constant, and  $C$  represents the fraction of the total generated power by the reheating process.

**2.2. Generators**

Generators are devices used to convert mechanical energy from the turbine into electrical energy [23]. The generator’s transfer function is given by (3)

$$G_p(s) = \frac{K_p}{1 + sT_p} \tag{3}$$

where  $G_p$  represents the generated power,  $K_p$  represents the electric system gain and  $T_p$  is the electric system time constant

**2.3. Governors**

Governors are used to measure and regulating the speed of a machine, i.e., they maintain the stability of the turbine or the speed of the generator [28]. The governor changes the turbine input if it senses the deviation in frequency due to a variation in load [23]. The transfer function of the governor is given in (4)

$$\frac{\Delta P_v(s)}{\Delta P_g(s)} = \frac{1}{1 + sT_g} \tag{4}$$

where  $\Delta P_v(s)$  represents the output from the generator,  $\Delta P_g(s)$  indicates input to the generator and  $T_g$  is the time constant of the governor.

**2.4. Tie-Lines**

Transmission lines are used in the power system to connect an area to its neighboring area, thereby allowing the exchange of power between these areas. A multi-area power system network comprises at least two areas that are linked together by transmission lines. Each area within the system has three inputs, i.e.,  $\Delta P_{ref}$  which is denoted as  $U_{ref}$ ,  $\Delta P_D$  which is the load disturbance in the area and  $\Delta P_{tie}$  which represents the transmission line power error [4]. Fig. 1 shows the block diagram of a multi-area power system network for control area  $i$ .

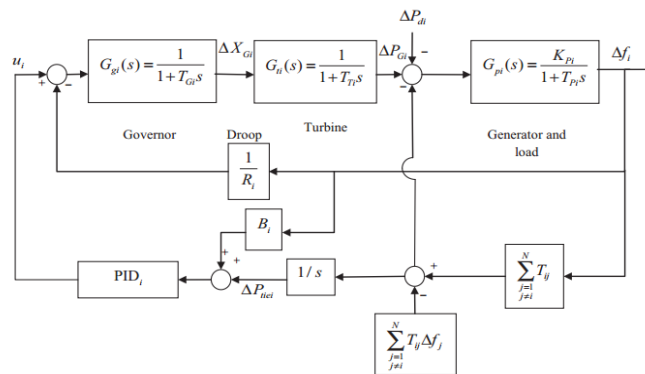


**Fig. 1.** The block diagram of control area  $i$  (Anwar and Pan [4])

**2.5. Area Control Error**

Area Control Error (ACE) is the difference between schedule and actual generated power within an area taking into account the frequency bias factor [24]. The ACE of an area is used in LFC to

maintain the frequency of that area very close to the defined values and the tie-line power exchange very close to its scheduled value. When the ACE of an area is zero, the frequency deviation and the tie-line power of that area will also be set to zero [13]. Area control error can be mathematically modeled by (5)

$$ACE = \sum_{k+1}^k P_k - P_s + B (f_{act} - f_0)MW \quad (5)$$

where  $P_k$  represents the tie-line power,  $P_s$  is the scheduled power exchange,  $f_0$  is the base frequency,  $f_{act}$  is the actual frequency, and  $B$  is the frequency bias coefficient.

When the ACE is negative, it indicates that the power flows out of an area is either very small or there is a drop in frequency or both. As such, the generation has to be increased [42].

### 3. Fractional Order PID Controller

#### 3.1. Fractional Calculus and Fractional Order Controller

The fractional Order PID (FOPID) controller is an extension of the PID controller with additional fractional integral and derivative choices [3]. The FOPID transfer function is given in (6).

$$C(s) = K_p + \left(\frac{K_i}{s^\lambda}\right) + K_d s^\mu \quad (6)$$

where the proportional gain is represented by  $K_p$ , the integral gain is represented by  $K_i$ ,  $K_d$  is the derivative gain,  $\mu$  is the fractional part of the derivative gain, and  $\lambda$  represents the fractional part of the integral gain.

The fractional order PID controller has five tuning parameters, i.e., the PID controller knobs:  $K_p$ ,  $K_i$  and  $K_d$ , and the fractional part of the integral and derivative gain  $\lambda$ , and  $\mu$ , respectively. The PID controllers are specific to 5 cases of the FOPID controller. When  $\lambda = \mu = 1$ , an Integer Order PID controller is obtained. When  $\lambda = \mu = 0$ , an integer order promotional controller is obtained. When  $\lambda = 0$  and  $\mu = 1$ , an Integer Order promotional derivative controller is obtained, and for  $\lambda = 1$  and  $\mu = 0$ , an Integer Order proportional-integral controller is obtained. Since the integer order, the PID controller has two fewer tuning parameters than the FOPID, the FOPID controller gives a better chance to design a more robust controller than the IOPID controller, particularly when a fractional system is to be controlled [25][47]. The structure of the FOPID controller is given in Fig. 2.

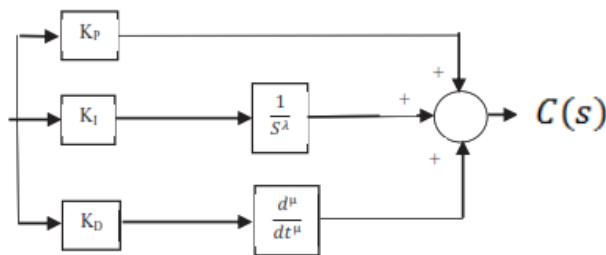


Fig. 2. FOPID controller

## 4. Method

### 4.1. Ant Lion Optimizer

Ant Lion Optimizer Algorithm (ALO) mimics the interaction between antlions and ants in a trap [26]. To model such interactions, ants are required to move over the search space, and antlions are

allowed to hunt them and become fitter using traps [35]. The antlion digs a cone-shaped pit in the sand by moving along a circular path and throwing out sand with its massive jaw [26]. Different cone-shaped pits dogged by the antlion are shown in Fig. 3. After digging the trap, the antlion hides beneath the bottom of the cone and waits for insects to be trapped in the pit, as illustrated in Fig. 4 [26].



Fig. 3. Different sizes of cone-shaped pits (Mirjalili [26])

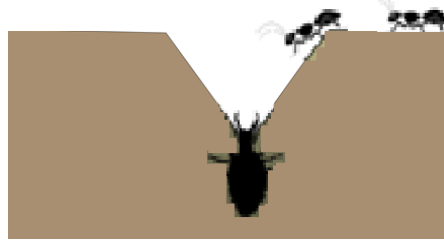


Fig. 4. The antlion is positioned at the bottom of the cone (Mirjalili [26])

In order to have the ants trapped in the pit, the edges of the trap are made sharp, and the slopes very steep. The antlion immediately tries to catch any ant that falls into the trap. When the prey (Ants) tries to escape from the antlion (Predator) pit, the antlion intelligently throws sand to the edges of the pit using its jaws. This is done so as to draw the ant back to the bottom of the pit [26]. The antlion draws the Ant inside the soil and consumes the prey. The antlion then throws out the remains and rebuilds the trap for the next catch.

#### 4.2. The Operators in ALO Algorithm

Ants search for food by moving randomly. Such movements can be modeled using (7) [26].

$$X(t) = [0, cs(2r(t_1) - 1), cs(2r(t_2) - 1), \dots, cs(2r(t_n) - 1)] \quad (7)$$

The cumulative sum is represented by  $cs$ , the maximum number of iterations is represented by  $n$ ,  $t$  represents a step of a random walk and  $r(t)$  represents random function given in (8)

$$r(t) = \begin{cases} 1 & \text{if } rand > 0.5 \\ 0 & \text{if } rand \leq 0.5 \end{cases} \quad (8)$$

where  $rand$  is a random number generated with uniform distribution in the interval of  $[0, 1]$

#### 4.3. Description of Random Walks by Ants

Since ants update their location using random walks at each optimization step, it is required to keep the random walks within the search area, (9) will be used at each step of optimization for normalization [26]

$$X_{norm} = \frac{(x(t) - a_i) \times (d_i^t - c_i^t)}{(b_i^t - a_i) + c_i} \quad (9)$$

where  $X_{norm}$  represent the normalized random walk, the minimum random walk of  $i - th$  variable is represented by  $a_i$ , the maximum random walk of  $i - th$  variable is represented by  $d_i$ ,  $x(t)$  is the random walk of Ant,  $c_i^t$  represents the minimum of  $i - th$  variable at  $t - th$  iteration,  $d_i^t$  indicates the maximum of  $i - th$  variable at  $t - th$  iteration and  $c_i$  is the minimum of the  $i - th$  variable. Equation (9) is used so as to guarantee all the stochastic movement of an ant inside the search space.

#### 4.4. Trapping prey in Antlion's Pits

Ants walk randomly within the search space while the antlion walks in a circular form inside its pit. The antlion uses this circular movement to attract ants to the trap. The scenario that describes the trapping of ants within the antlion's pit is influenced by the random movement of the ant. This scenario is modeled using (10) and (11) [26]

$$c_j^t = Antlion_j^t + c^t \quad (10)$$

$$d_j^t = Antlion_j^t + d^t \quad (11)$$

where the minimum variables at  $t - th$  iteration are represented by  $c^t$ , the vector, including the maximum of all variables at  $t - th$  iteration, is represented by  $d^t$ , the minimum variable for  $j - th$  ant at  $t - th$  iteration is represented by  $c_j^t$ , the maximum variables for  $j - th$  ant at  $t - th$  iteration is represented by  $d_j^t$  and  $Antlion_j^t$  represents the position of the selected  $j - th$  antlion at the  $t - th$  iteration.

#### 4.5. Process of Sliding Ants towards the Antlion

Antlion throws sand toward the middle of the trap as it realizes an ant is inside the pit. Such behavior prevents an ant from escaping from the trap. To model this behavior mathematically, (12) and (13) are proposed [26].

$$c^t = \frac{c^t}{I} \quad (12)$$

$$d^t = \frac{d^t}{I} \quad (13)$$

where  $I$  represents a ratio, the minimum variable at  $t - th$  iteration is represented by  $c^t$ , the vector containing the maximum variables at the  $t - th$  iteration is represented by  $d^t$ . From (12) and (13),  $= 10^w \frac{t}{T}$ , as  $t$  stands for the current iteration, maximum number of iterations is represented by  $T$ , and  $w$  represent a constant defined by the current iteration.

#### 4.6. Process of Catching the Prey in the Trap and Re-building the Trap

In order to model the process by which an ant is pulled into the soil and consumed by an antlion when it tries to escape, it is assumed that the antlion is fitter than the corresponding ant. The antlion needs to relocate to the position of the ant being hunted, which will give it a better chance of catching new ants. Equation (14) is used to model such behavior [26].

$$Antlion_j^t = Ant_j^t \quad \text{if} \quad (Ant_j^t) > f(Antlion_j^t) \quad (14)$$

where  $t$  is the current iteration,  $Antlion_j^t$  stands for the position of selected  $j - th$  antlion at the  $t - th$  iteration, and  $Ant_j^t$  represents the position of  $j$ -th Ant at  $t - th$  iteration.

#### 4.7. Elitism

The phenomenon that describes the characteristics of the evolutionary algorithm that enable it to retain the best solution (s) obtained at any stage of the optimization process is called Elitism [26]. For every scenario, the antlion with the best fitness is noted and regarded as elite. The movement of all

ants during iterations is expected to be influenced by the elite. In this case, the antlion is expected to guide all ants toward the promising region on the search space by moving randomly using the roulette wheel and the elite. This behavior can be mathematically modeled using (15):

$$Ant_j^t = \frac{R_A^t + R_E^t}{2} \quad (15)$$

where  $R_A^t$  represents the stochastic walk around the antlion at the  $t$ -th iteration,  $R_E^t$  represents random walk around the elite at  $t$ -th iteration and  $Ant_j^t$  represents the position of  $i$ -th ant at  $t$ -th iteration. The ant lion optimizer algorithm pseudocode is defined in Table 1.

**Table 1.** Pseudocode of ALO algorithm

S/N	Steps
1.	Initialize the initial population of antlions and ants randomly
2.	Compute the fitness of antlions and ants
3.	Locate the best antlions and consider it as the elite
4.	(determined optimum)
5.	<b>while</b> the final list is not mollified
6.	<b>for</b> all ant
7.	Choose an antlion by means of a Roulette wheel
8.	Update c and d using (12) and (13)
9.	Create and normalize random walks using (7) and (8)
10.	Update the location of the ant using (15)
11.	end for
12.	Compute all the ant's fitness
13.	Substitute an antlion with its equivalent ant when the ant
14.	becomes fitter (14)
15.	Update elite if an antlion gets fitter than the elite
16.	end while
17.	<b>Return</b> elite

#### 4.8. Optimizing the Gains of FOPID Controller

In this section, the gains of the Fractional Order PID controller will be optimized using the ant lion optimizer. This will be done by linking the designed Simulink model to the ant lion optimizer algorithm using the “Sim” command. The objective function to be minimized for the four-area power system is the Integral Square Error (ISE) given by (16). The errors that form the ISE to be minimized are frequency deviation, tie-line power deviation and area control error.

$$ISE = \int_0^t \left( \begin{array}{l} (f_1)^2 + (f_2)^2 + (f_3)^2 + (f_4)^2 + \\ (P_{t1})^2 + (P_{t2})^2 + (P_{t3})^2 + (P_{t4})^2 + \\ (ACE_1)^2 + (ACE_2)^2 + (ACE_3)^2 \\ +(ACE_4)^2 \end{array} \right) dt \quad (16)$$

where  $f_1$  represent the frequency deviation for area one,  $f_2$ , represent the frequency deviation for area two,  $f_3$ , is the frequency deviation for area three,  $f_4$  represent the frequency deviation for area four,  $P_{t1}$  is the tie-line power deviation that link area one and two,  $P_{t2}$  is the tie-line power deviation that link area two and three,  $P_{t3}$  represent the tie-line power deviation that link area three and four,  $P_{t4}$  is the tie-line power deviation that link area four and one,  $ACE_1$  is the Area Control Error for area one,  $ACE_2$  represent the Area Control Error for area two  $ACE_3$  represent the Area Control Error for area three,  $ACE_4$  represent the Area Control Error for area four, and  $t$  is the simulation time.

The simulation parameters of the ant lion optimizer algorithm are given in Table 2. The simulation parameters in Table 2 are used to determine the optimal gain of the proposed FOPID controller. The lower bound (lb) and the upper bound (ub) vary depending on the gain of the FOPID controller to be optimized. When optimizing the fractional part of the controller, i.e., lambda and mu

( $\lambda$  and  $\mu$ ), the lower bound was set to 0.5, and the upper bound was set to 1.1. However, when optimizing the gain of the integer part of the controller, i.e., Proportional, Integral and Derivative (PID), the lower bound was set to 0.1, and the upper bound was set to 200.

**Table 2.** Ant lion optimizer algorithm simulation parameters

SN	Parameters	Symbol	Value
1	Number of search agents	SearchAgents_no	250
2	Number of variables	Dim	5
3	Maximum number of iterations	Max_iteration	100
4	The lower bound (Kp, Ki, Kd)	Lb	0.1
5	Upper bound (Kp, Ki, Kd)	Ub	50
6	Lower bound ( $\lambda$ , $\mu$ )	lb	0.5
7	Upper bound ( $\lambda$ , $\mu$ )	ub	1.1

## 5. Simulations, Results and Discussion

### 5.1. Simulation for the Four-Area Power System

In the four-area thermal power system given in Fig. 5, areas one to area three is reheat thermal power plant, whereas area four is a non-reheat thermal power plant. The system parameters for areas one to three are:  $K_{p1} = K_{p2} = K_{p3} = 120$ ,  $T_{p1} = T_{p2} = T_{p3} = 20$ ,  $T_{t1} = T_{t2} = T_{t3} = 0.3$ ,  $T_{g1} = T_{g2} = T_{g3} = 0.08$ ,  $R_1 = R_2 = R_3 = 2.4$ ,  $B_1 = B_2 = B_3 = 0.425$ ,  $c_1 = c_2 = c_3 = 0.35$ ,  $T_{r1} = T_{r2} = T_{r3} = 4.2$ . The system parameters for area four are:  $K_{p4} = 120$ ,  $T_{p4} = 20$ ,  $T_{t4} = 0.3$ ,  $T_{g4} = 0.08$ ,  $R_4 = 2.4$ , and  $B_4 = 0.425$ . The tie-line coefficient for each area is  $T_{12} = T_{23} = T_{31} = T_{41} = 0.0707$ .

From Fig. 6, the step change in load disturbance of 0.01pu was applied to area one at time  $t = 5s$ , and the step change in load disturbance of 0.01pu was applied to area three at time  $t=100s$ . The frequency deviation for area one, area two, area three and area four are given in Fig. 7, Fig. 9, Fig. 11 and Fig. 13, respectively. To clearly see the signals, the zoom plot for the frequency deviation for area one, area two, area three and area four are given in Fig. 8, Fig. 10, Fig. 12 and Fig. 14, respectively. The tie-line power deviation for area one, area two, area three and area four are given in Fig. 15, Fig. 17, Fig. 19 and Fig. 21. To clearly see the signals, the zoom plot for the tie-line power deviation for area one, area two, area three and area four are given in Fig. 16, Fig. 18, Fig. 20 and Fig. 22 respectively. The peak value of the frequency deviation, settling time and ISE are not presented due to the limitation of space. However, the FOPID controller gains for the non-reheat thermal power system for areas one, two and three are:  $K_p = 26.02$ ,  $K_i = 5.78$ ,  $K_d = 5.5$ ,  $\lambda = 0.98$  and  $\mu = 0.92$ . The FOPID controller gain for the reheat thermal power system for area four are:  $K_p = 4.552$ ,  $K_i = 5.952$ ,  $K_d = 1.176$ ,  $\lambda = 0.98$  and  $\mu = 0.92$ .

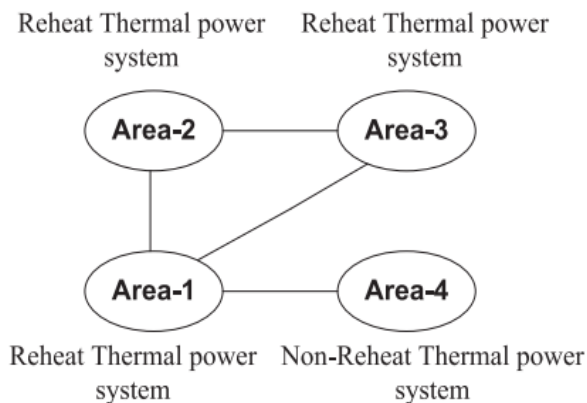


**Fig. 5.** Block diagram of the four-area thermal power system

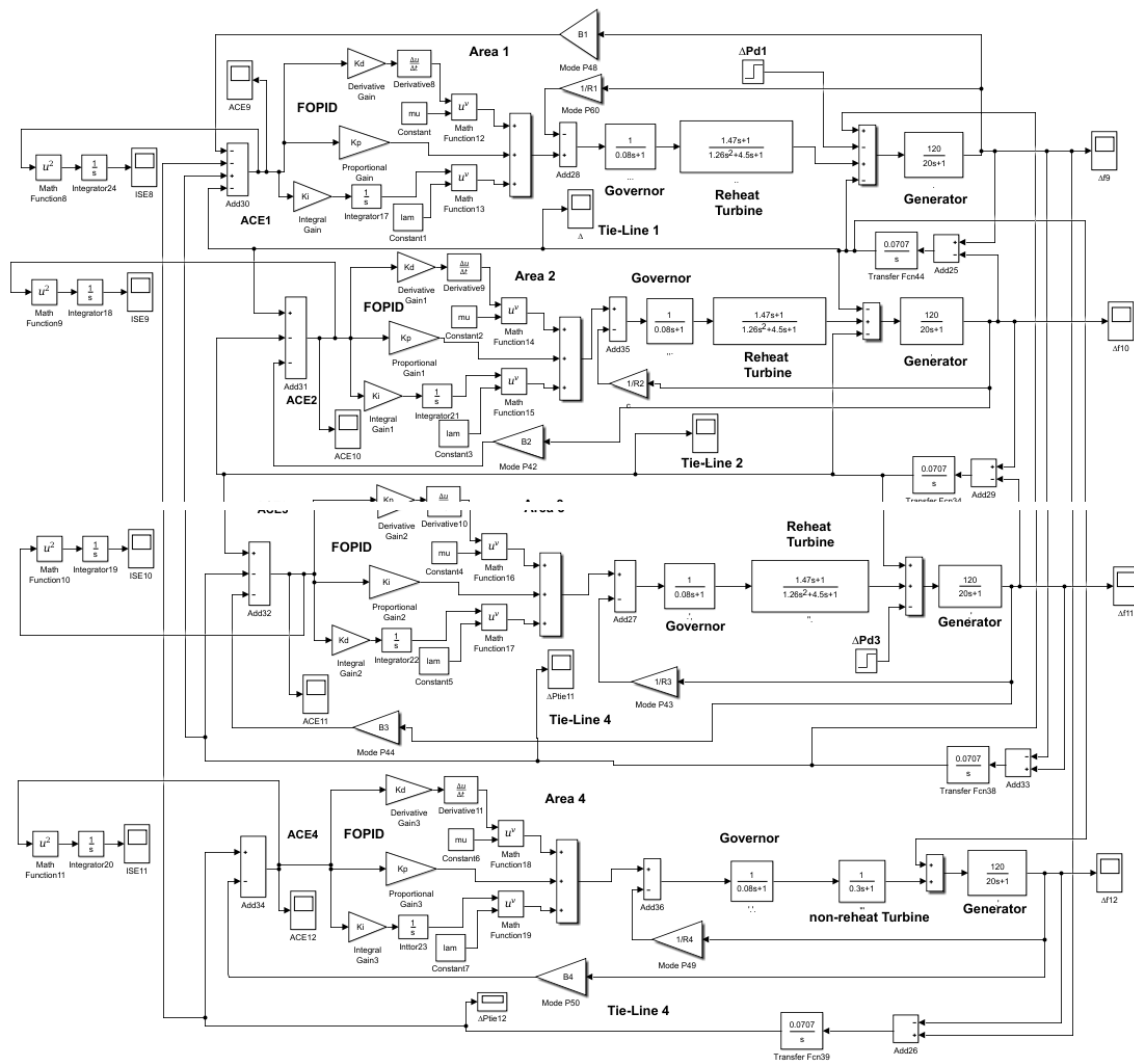


Fig. 6. Simulink Model of the four-area thermal power system

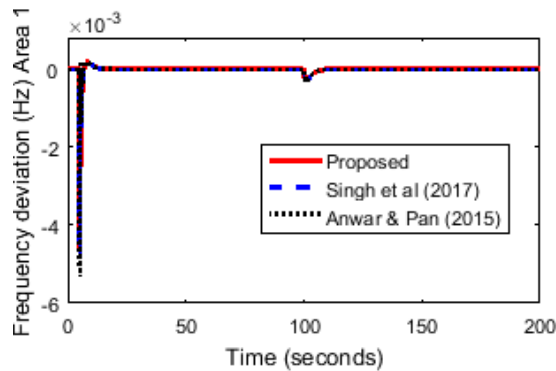


Fig. 7. Frequency deviation for area one

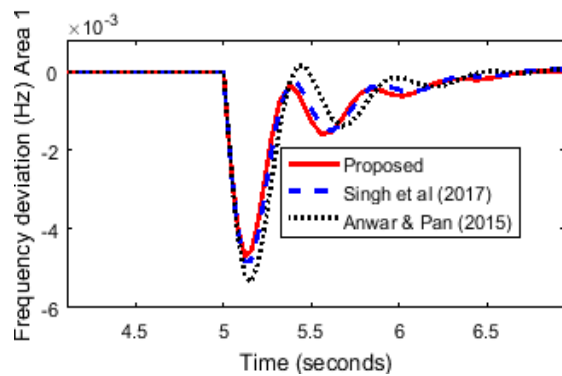


Fig. 8. Zoom plot for the frequency deviation of the area one at t=5sec

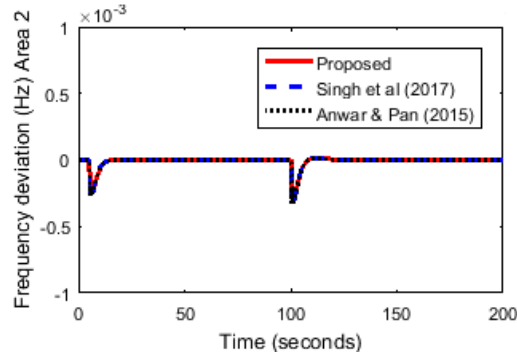


Fig. 9. Frequency deviation for area two

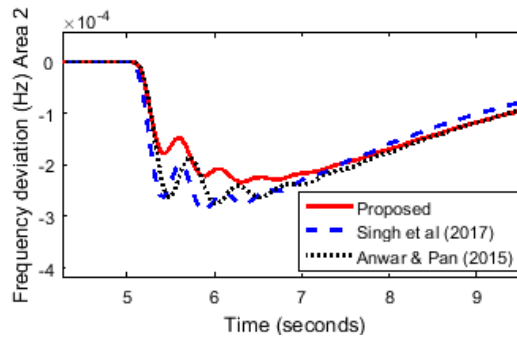


Fig. 10. Zoom plot for the frequency deviation of area two at t=5sec

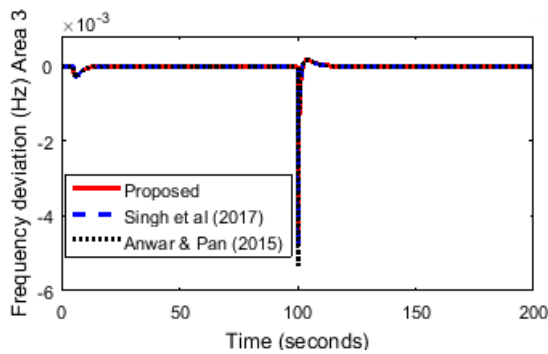


Fig. 11. Frequency deviation for area three

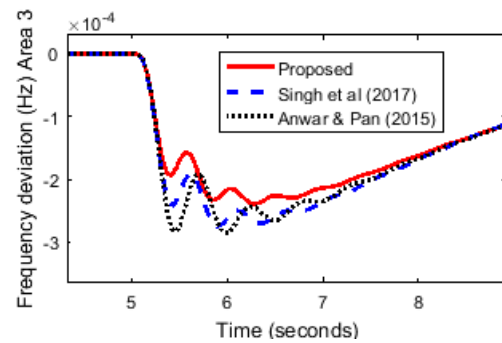


Fig. 12. Zoom plot for the frequency deviation of area three at t=5sec

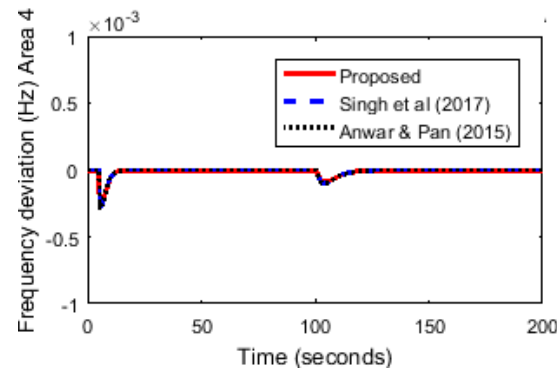


Fig. 13. Frequency deviation for area four

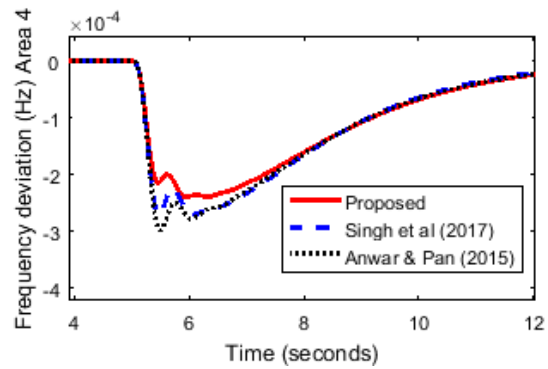


Fig. 14. Zoom plot for the frequency deviation of area four at t=5sec

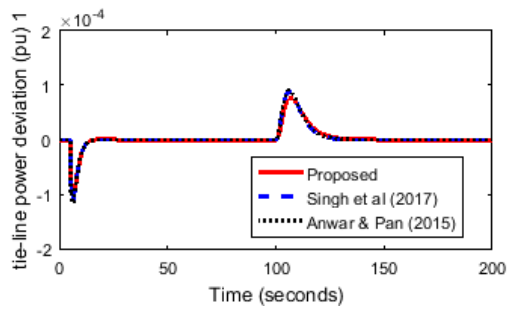


Fig. 15. Tie-line power deviation between areas one and two ( $T_{12}$ )

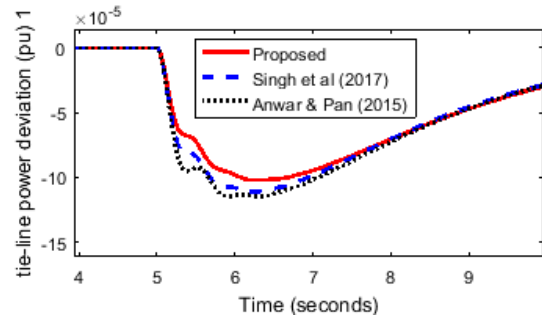


Fig. 16. Zoom plot of Tie-line power deviation  $T_{12}$  at  $t=5$ sec

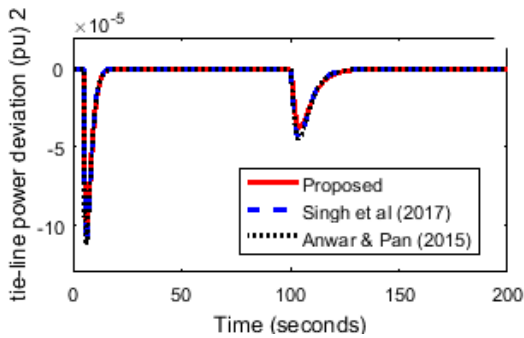


Fig. 17. Tie-line power deviation between areas two and three ( $T_{23}$ )

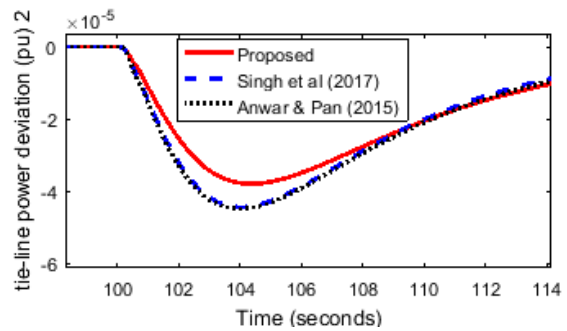


Fig. 18. Zoom plot of Tie-line power deviation  $T_{23}$  at  $t=5$ sec

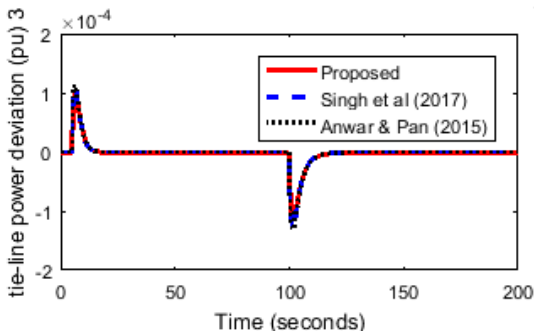


Fig. 19. Tie-line power deviation between areas three and one ( $T_{31}$ )

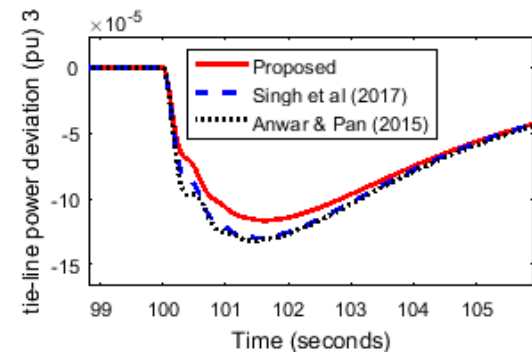


Fig. 20. Zoom plot of Tie-line power deviation  $T_{31}$  at  $t=5$ sec

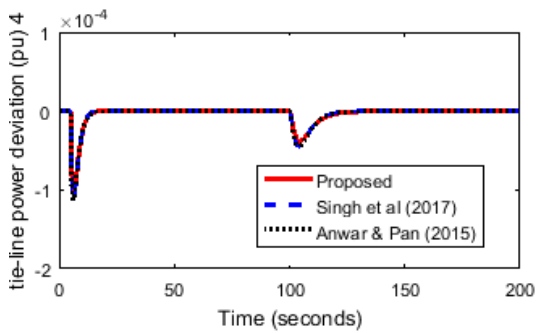


Fig. 21. Tie-line power deviation between areas four and one ( $T_{41}$ )

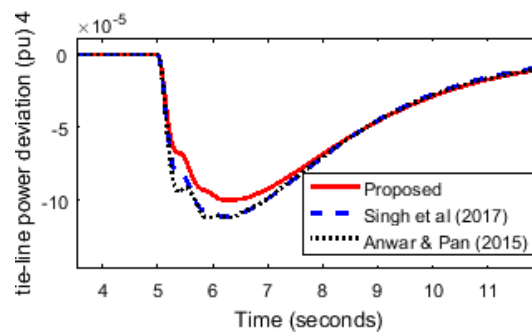


Fig. 22. Zoom plot of Tie-line power deviation  $T_{41}$  at  $t=5$ sec

The frequency deviation plots are given in Fig. 7 to Fig. 14, whereas the tie-line power deviation plots are given in Fig. 15 to Fig. 22. From Fig. 7 to Fig. 14, undershoot denotes that the load demand is greater than the generated power, whereas Overshoot denotes that the load demand is greater than the generated power whereas. From Fig. 15 to Fig. 22, undershoot denotes that the scheduled power is larger than the actual power, whereas overshoot denotes that the actual power is more than the scheduled power.

## 5.2. Discussion of Results

The result in Table 3-Table 10 shows the comparative analysis of the proposed method and the controllers designed by Singh et al. [2], Anwar and Pan [4]. From Table 3, the results showed that the modified FOPID controller was able to mitigate frequency deviation better than the controllers designed by Singh et al. [2] and Anwar and Pan [4]. The controller designed by Singh et al. [2] is the closest in performance to the modified FOPID controller. From Table 3, Table 4, Table 5 and Table 6, at  $t=5s$ , the load demand is greater than the generated power (undershoot) for areas one, two, three and four by  $-4.69 \times 10^{-3}Hz$ ,  $-0.2337 \times 10^{-3}Hz$ ,  $-0.2393 \times 10^{-3}Hz$  and  $-0.2392 \times 10^{-3}Hz$  respectively, for the modified FOPID. From Table 3, Table 4, Table 5 and Table 6, at  $t=5s$ , the load demand is greater than the generated power (undershoot) for areas one, two, three and four by  $-4.83 \times 10^{-3}Hz$ ,  $-0.2884 \times 10^{-3}Hz$ ,  $-0.2755 \times 10^{-3}Hz$  and  $-0.2702 \times 10^{-3}Hz$  respectively, for the designed method by Singh et al. [2]. This shows an improvement of 2.8%, 19%, 13.1% and 11.5% in reducing the error between the generated power and load demand for areas one, two, three and four, respectively, by the modified FOPID controller.

From Table 3, Table 4, Table 5 and Table 6, at  $t=5s$ , the time taken to balance the generated power and load demand (settling time) for areas one, two, three and four is 14.2s, 13.5s, 10.3s and 15.3s respectively, for the modified FOPID. From Table 3, Table 4, Table 5 and Table 6, at  $t=5s$ , the time taken to balance the generated power and load demand (settling time) for areas one, two, three and four is 15.7s, 14.2s, 11.5s and 16.2s respectively, for the designed method by Singh et al. [2]. This shows that the modified FOPID controller was able to balance the generated power and load demand faster than the designed method by Singh et al. [2].

From Table 3, Table 4, Table 5 and Table 6, at  $t=100s$ , the load demand is greater than the generated power (undershoot) for areas one, two, three and four by  $-0.255 \times 10^{-3}Hz$ ,  $-0.2816 \times 10^{-3}Hz$ ,  $-4.744 \times 10^{-3}Hz$  and  $-0.0879 \times 10^{-3}Hz$  respectively, for the modified FOPID. From Table 3, Table 4, Table 5 and Table 6, at  $t=100s$ , the load demand is greater than the generated power (undershoot) for areas one, two, three and four by  $-0.291 \times 10^{-3}Hz$ ,  $-0.3164 \times 10^{-3}Hz$ ,  $-4.912 \times 10^{-3}Hz$  and  $-0.0989 \times 10^{-3}Hz$  respectively, for the designed method by Singh et al. [2]. This shows an improvement of 12.4%, 11%, 3.4% and 11.1% in reducing the error between the generated power and load demand for areas one, two, three and four, respectively, by the modified FOPID controller.

From Table 3, Table 4, Table 5 and Table 6, at  $t=100s$ , the time taken to balance the generated power and load demand (settling time) for areas one, two, three and four is 110s, 118s, 111s and 126s, respectively, for the modified FOPID. From Table 3, Table 4, Table 5 and Table 6, at  $t=100s$ , the time taken to balance the generated power and load demand (settling time) for areas one, two, three and four is 111s, 119s, 112s and 128s, respectively, for the designed method by Singh et al. [2]. This shows that the modified FOPID controller was able to balance the generated power and load demand faster than the designed method by Singh et al. [2].

From Table 7, Table 8 and Table 10, at  $t=5s$ , the scheduled power is larger than the actual power (undershoot) for tie-lines one, two and four by  $-1.022 \times 10^{-4}Hz$ ,  $-1.001 \times 10^{-4}Hz$  and  $-1.001 \times 10^{-4}Hz$  respectively, for the modified FOPID. From Table 9, at  $t=5s$ , the actual power is more than the scheduled power (overshoot) for tie-line three by  $1.012 \times 10^{-4}Hz$ , for the modified FOPID. From Table 7, Table 8 and Table 10, at  $t=5s$ , the scheduled power is larger than the actual power (undershoot) for tie-lines one, two and four by  $-1.114 \times 10^{-4}Hz$ ,  $-1.119 \times 10^{-4}Hz$  and  $-1.119 \times 10^{-4}Hz$  respectively, for the designed method by Singh et al. [2]. From Table 9, at  $t=5s$ ,

the actual power is more than the scheduled power (overshoot) for tie-line three by  $1.128 \times 10^{-4} \text{ Hz}$ , for the designed method by Singh et al. [2]. This shows an improvement of 8.3%, 10.5%, 10.3% and 10.5% in reducing the error between the schedule and actual power in tie-lines one, two, three and four, respectively, by the modified FOPID controller.

From Table 7, Table 8, Table 9 and Table 10, at  $t=5\text{s}$ , the time taken to balance the generated power and load demand (settling time) for areas one, two, three and four is 14.5s, 16s, 13.8s and 14s, respectively, for the modified FOPID. From Table 7, Table 8, Table 9 and Table 10, at  $t=5\text{s}$ , the time taken to balance the generated power and load demand (settling time) for areas one, two, three and four is 15s, 16.7s, 15s and 15s, respectively, for the designed method by Singh et al. [2]. This shows that the modified FOPID controller was able to balance the generated power and load demand faster than the designed method by Singh et al. [2] in tie-lines one, two, three and four at  $t=5\text{s}$ .

From Table 9, at  $t=100\text{s}$ , the actual power is more than the scheduled power (overshoot) for tie-line three by  $0.1085 \times 10^{-4} \text{ Hz}$ , for the modified FOPID. From Table 7, Table 8 and Table 10, at  $t=100\text{s}$ , the scheduled power is larger than the actual power (undershoot) for tie-lines one, two and four by  $-0.3783 \times 10^{-4} \text{ Hz}$ ,  $-1.165 \times 10^{-4} \text{ Hz}$  and  $-0.3783 \times 10^{-4} \text{ Hz}$  respectively, for the modified FOPID. From Table 9, at  $t=100\text{s}$ , the actual power is more than the scheduled power (overshoot) for tie-line three by  $0.126 \times 10^{-4} \text{ Hz}$ , for the designed method by Singh et al. [2]. From Table 7, Table 8 and Table 10, at  $t=100\text{s}$ , the scheduled power is larger than the actual power (undershoot) for tie-lines one, two and four by  $-0.4439 \times 10^{-4} \text{ Hz}$ ,  $-1.298 \times 10^{-4} \text{ Hz}$  and  $-0.4439 \times 10^{-4} \text{ Hz}$  respectively, for the designed method by Singh et al. [2]. This shows an improvement of 14.9%, 10.2%, 13.5% and 14.9% in reducing the error between the schedule and actual power in tie-lines one, two, three and four, respectively, by the modified FOPID controller.

From Table 7, Table 8, Table 9 and Table 10, at  $t=100\text{s}$ , the time taken to balance the generated power and load demand (settling time) for areas one, two, three and four is 123s, 132.6s, 122s and 124.2s respectively, for the modified FOPID. From Table 7, Table 8, Table 9 and Table 10, at  $t=100\text{s}$ , the time taken to balance the generated power and load demand (settling time) for areas one, two, three and four is 124s, 133s, 123s and 125s, respectively, for the designed method by Singh et al. [2]. This shows that the modified FOPID controller was able to balance the generated power and load demand faster than the designed method by Singh et al. [2] in tie-lines one, two, three and four at  $t=100\text{s}$ .

In general, the modified FOPID was able to minimize frequency deviation better than the controllers designed by Singh et al. [2] and Anwar and Pan [4]. This was a result of the additional tuning knobs ( $\lambda$  and  $\mu$ ) in the fraction order PID controller. The modified FOPID controller was also able to balance the error between the scheduled and actual power faster than the controllers designed by Singh et al. [2] and Anwar and Pan [4].

**Table 3.** Comparative analysis for area one

Method	Controller gains $Kp; Ki; Kd; \lambda; \mu$	Area one at Time $t=5\text{s}$			Area one at time $t=100\text{s}$		
		Frequency deviation ( $\times 10^{-3}$ ) Hz	Settling time (s)	ISE ( $\times 10^{-5}$ )	Frequency deviation ( $\times 10^{-3}$ ) Hz	Settling time (s)	ISE ( $\times 10^{-9}$ )
<b>Proposed FOPID</b>	26.02; 5.78; 5.5; 0.98; 0.92	-4.69	14.2	0.1173	-0.255	110	0.1173
Singh et al. [1]	25.103; 6.112; 5.23; -; -	-4.83	15.7	0.1285	-0.291	111	0.1285
Anwar & Pan [4]	24.941; 5.88; 5.48; -; -	-5.34	15.7	0.1478	-0.3171	111	0.1478

**Table 4.** Comparative analysis for area two

Method	Controller gains $Kp; Ki; Kd; \lambda; \mu$	Area two at Time $t=5\text{s}$			Area two at time $t=100\text{s}$		
		Frequency deviation ( $\times 10^{-3}$ ) Hz	Settling time (s)	ISE ( $\times 10^{-9}$ )	Frequency deviation ( $\times 10^{-3}$ ) Hz	Settling time (s)	ISE ( $\times 10^{-9}$ )
<b>Proposed FOPID</b>	26.02; 5.78; 5.5; 0.98; 0.92	-0.2337	13.5	0.502	-0.2816	118	0.502
Singh et al. [1]	25.103; 6.112; 5.23; -; -	-0.2884	14.2	0.591	-0.3164	119	0.591
Anwar & Pan [4]	24.941; 5.88; 5.48; -; -	-0.2767	14.5	1.168	-0.3366	119	1.168

**Table 5.** Comparative analysis for area three

Method	Controller gains $Kp; Ki; Kd; \lambda; \mu$	Area three at Time t=5s			Area three at time t=100s		
		Frequency deviation ( $\times 10^{-3}$ ) Hz	Settling time (s)	ISE ( $\times 10^{-5}$ )	Frequency deviation ( $\times 10^{-3}$ ) Hz	Settling time (s)	ISE ( $\times 10^{-5}$ )
<b>Proposed FOPID</b>	<b>26.02; 5.78; 5.5; 0.98; 0.92</b>	<b>-0.2393</b>	<b>10.3</b>	<b>0.1168</b>	<b>-4.744</b>	<b>111</b>	<b>0.1168</b>
Singh et al. [1]	25.103; 6.112; 5.23; -; -	-0.2755	11.5	0.1278	-4.912	112	0.1278
Anwar & Pan [4]	24.941; 5.88; 5.48; -; -	-0.2851	11.5	0.1464	-5.322	112	0.1464

**Table 6.** Comparative analysis for area four

Method	Controller gains $Kp; Ki; Kd; \lambda; \mu$	Area four at Time t=5s			Area four at time t=100s		
		Frequency deviation ( $\times 10^{-3}$ ) Hz	Settling time (s)	ISE ( $\times 10^{-9}$ )	Frequency deviation ( $\times 10^{-3}$ ) Hz	Settling time (s)	ISE ( $\times 10^{-9}$ )
<b>Proposed FOPID</b>	<b>26.02; 5.78; 5.5; 0.98; 0.92</b>	<b>-0.2392</b>	<b>15.3</b>	<b>0.0179</b>	<b>-0.0879</b>	<b>126</b>	<b>0.0179</b>
Singh et al. [1]	25.103; 6.112; 5.23; -; -	-0.2702	16.2	0.3739	-0.0989	128	0.3739
Anwar & Pan [4]	24.941; 5.88; 5.48; -; -	-0.2991	20.8	0.4695	-0.1038	128	0.4695

**Table 7.** Comparative analysis for the tie-line that connect area one to two ( $T_{12}$ )

Method	Controller gains $Kp; Ki; Kd; \lambda; \mu$	$T_{12}$ at Time t=5s			$T_{12}$ at time t=100s		
		Frequency deviation ( $\times 10^{-4}$ ) Hz	Settling time (s)	ISE ( $\times 10^{-7}$ )	Frequency deviation ( $\times 10^{-4}$ ) Hz	Settling time (s)	ISE ( $\times 10^{-7}$ )
<b>Proposed FOPID</b>	<b>26.02 5.78 5.5 0.98 0.92</b>	<b>1.022</b>	<b>14.5</b>	<b>0.2909</b>	<b>-0.1083</b>	<b>123</b>	<b>0.2909</b>
Singh et al. [1]	25.103 6.112 5.23 - -	1.114	15	0.3241	-0.126	124	0.3241
Anwar & Pan [4]	24.941 5.88 5.48 - -	1.151	25	0.3518	-0.129	124	0.3518

**Table 8.** Comparative analysis for the tie-line that connect area two to three ( $T_{23}$ )

Method	Controller gains $Kp; Ki; Kd; \lambda; \mu$	$T_{23}$ at Time t=5s			$T_{23}$ at time t=100s		
		Frequency deviation ( $\times 10^{-4}$ ) Hz	Settling time (s)	ISE ( $\times 10^{-7}$ )	Frequency deviation ( $\times 10^{-4}$ ) Hz	Settling time (s)	ISE ( $\times 10^{-7}$ )
<b>Proposed FOPID</b>	<b>26.02; 5.78; 5.5; 0.98; 0.92</b>	<b>1.001</b>	<b>16</b>	<b>0.413</b>	<b>-0.3783</b>	<b>132.6</b>	<b>0.413</b>
Singh et al. [1]	25.103; 6.112; 5.23; -; -	1.119	16.7	0.4804	-0.4439	133	0.4808
Anwar & Pan [4]	24.941; 5.88; 5.48; -; -	1.121	21	0.5004	-0.4482	133	0.5004

**Table 9.** Comparative analysis for the tie-line that connects areas three to four ( $T_{34}$ )

Method	Controller gains $Kp; Ki; Kd; \lambda; \mu$	$T_{34}$ at Time t=5s			$T_{34}$ at time t=100s		
		Frequency deviation ( $\times 10^{-4}$ ) Hz	Settling time (s)	ISE ( $\times 10^{-7}$ )	Frequency deviation ( $\times 10^{-4}$ ) Hz	Settling time (s)	ISE ( $\times 10^{-7}$ )
<b>Proposed FOPID</b>	<b>26.02; 5.78; 5.5; 0.98; 0.92</b>	<b>1.012</b>	<b>13.8</b>	<b>0.7538</b>	<b>-1.165</b>	<b>122</b>	<b>0.7538</b>
Singh et al. [1]	25.103; 6.112; 5.23; -; -	1.128	15	0.8776	-1.297	123	0.8776
Anwar & Pan [4]	24.941; 5.88; 5.48; -; -	1.137	15	0.9187	-1.32	123	0.9187

**Table 10.** Comparative analysis for the tie-line that connects area four to one ( $T_{41}$ )

Method	Controller gains $Kp; Ki; Kd; \lambda; \mu$	$T_{41}$ at Time t=5s			$T_{41}$ at time t=100s		
		Frequency deviation ( $\times 10^{-4}$ ) Hz	Settling time (s)	ISE ( $\times 10^{-7}$ )	Frequency deviation ( $\times 10^{-4}$ ) Hz	Settling time (s)	ISE ( $\times 10^{-7}$ )
<b>Proposed FOPID</b>	<b>26.02; 5.78; 5.5; 0.98; 0.92</b>	<b>-1.001</b>	<b>14</b>	<b>0.3676</b>	<b>-0.3783</b>	<b>124.2</b>	<b>0.3676</b>
Singh et al. [1]	25.103; 6.112; 5.23; -; -	-1.119	15	0.4343	-0.4439	125	0.4343
Anwar & Pan [4]	24.941; 5.88; 5.48; -; -	-1.121	15	0.4487	-0.4482	125	0.4487

## 6. Conclusion and Further Works

In this paper, a modified fractional order PID controller to mitigate frequency deviation in a four-area power system has been presented. The gains of the proposed modified FOPID controller were optimized using the ant lion optimizer algorithm. The ant lion optimizer algorithm was linked to the four-area power system. The objective function for minimization was Integral Square Error (ISE), while the errors that were minimized were frequency deviation, tie-line power deviation and area control error. Simulations were carried out, and optimal values of the FOPID controller were obtained.

From the results obtained, the proposed modified FOPID controller outperformed the controllers designed by Singh et al. [2] and Anwar & Pan [4] in terms of frequency deviation, tie-line power deviation and area control error. Nonlinearities such as time delay, boiler dynamics, governor dead band and generation rate constraints exist in any practical power system. As such, studying the behavior of a real power system requires including these constraints in the power system design. As such, these nonlinearities can be included in a four-area power system for further research. This is required to improve the quality and reliability of the power system. Extending the combination of the physical constraints given above into a three or four-area power system becomes paramount in studying a real interconnected power system.

**Author Contribution:** All authors contributed equally to the main contributor to this paper. All authors read and approved the final paper.

**Funding:** This research received no external funding.

**Conflicts of Interest:** The authors declare no conflict of interest.

## References

- [1] A. M. Saba, "Fractional Order PID Controller for Minimizing Frequency Deviation in a Single and Multi-area Power System with Physical Constraints," *Journal of the Robotic and Control*, vol. 3, no. 1, 2022, <https://doi.org/10.18196/jrc.v3i1.11356>.
- [2] V. P. Singh, N. Kishor and P. Samuel, "Improved Load Frequency Control of Power System using LMI based PID approach," *Journal of the Franklin Institute*, vol. 354, pp. 6805-6830, 2017, <https://doi.org/10.1016/j.jfranklin.2017.08.031>.
- [3] R. Lamba, S. K. Singla, and S. Sondhi, "Design of fractional order PID controller for load frequency control in perturbed two area interconnected system," *Electric Power Components and Systems*, vol. 47, no. 11-12, pp. 998-1011, 2019, <https://doi.org/10.1080/15325008.2019.1660736>.
- [4] Md. N. Anwar and S. Pan, "A new PID Load Frequency Controller Design method in Frequency Domain through Direct Synthesis approach," *International Journal of Electrical Power and Energy Systems*, vol. 67, pp. 560- 569, 2015, <https://doi.org/10.1016/j.ijepes.2014.12.024>.
- [5] S. S. Aung and Z. M. Htike, "Modeling and Simulation of Load Frequency Control for Three Area Power System Using Proportional Integral Derivative (PID) Controller," *American Scientific Research Journal for Engineering, Technology, and Sciences (ASRJETS)*, vol. 26, no 2, pp. 301-315, 2016, <https://core.ac.uk/download/pdf/235050067.pdf>.
- [6] K. Lu, W. Zhou, G. Zeng, and Y. Zheng, "Constrained population extremal optimization-based robust load frequency control of multi-area interconnected power system," *International Journal of Electrical Power & Energy Systems*, vol. 105, pp. 249-271, 2019, <https://doi.org/10.1016/j.ijepes.2018.08.043>.
- [7] P. Balasundaram and C. I. Akilandam, "ABC Algorithm based Load- Frequency Controller for an interconnected Power System Considering nonlinearities and Coordinated with UPFC and RFB," *International Journal of Engineering and Innovative Technology (IJEIT)*, vol. 1, no. 3, pp. 234-255, 2012, [https://www.ijeit.com/vol%201/Issue%203/IJEIT1412201203\\_01.pdf](https://www.ijeit.com/vol%201/Issue%203/IJEIT1412201203_01.pdf).
- [8] S. P. Behera and A. Biswal, "Design and Analysis of TIDF controller in AGC with Thyristor Controlled series capacitor," *International Journal of Innovative Research in Electrical, Electronics, Instrumentation and Control Engineering*, vol. 5, no. 3, pp. 223-231, 2017, <https://doi.org/10.17148/IJIREICE.2017.5319>.
- [9] P. A. Gbadega and A. K. Saha, "Dynamic Tuning of the Controller Parameters in a Two-Area Multi-Source Power System for Optimal Load Frequency Control Performance," *International Journal of Engineering Research in Africa*, vol. 51, pp. 111-129, 2020, <https://doi.org/10.4028/www.scientific.net/JERA.51.111>.

- [10] J. Y. Cao and B. G. Cao, "Design of Fractional Order Controller Based on Particle Swarm Optimization," *International Journal of Control, Automation and Systems*, vol. 4, no. 6, pp. 775-781, 2006, <https://doi.org/10.1109/ICIEA.2006.257091>.
- [11] V. Celik, M. T. Ozdemir and G. Bayrak, "The effects on stability region of the fractional-order PI controller for one-area time-delayed load–frequency control systems," *Transactions of the Institute of Measurement and Control*, vol. 1, pp. 1–13, 2016, <https://doi.org/10.1177/0142331216642839>.
- [12] M. Chiranjeevi and V. S. G. Lakshmi, "Design of PSO based Fractional order Load Frequency controller for two area power system," *Journal of Electrical and Electronics Engineering (IOSR-JEEE)*, vol. 9, no. 6, pp. 67-74, 2014, <https://doi.org/10.9790/1676-09626774>.
- [13] A. Delassi, S. Arif and L. Mokrani, "Load frequency control problem in interconnected power systems using robust fractional PI<sup>λ</sup>D controller," *Ain Shams Engineering Journal*, vol. 1, pp. 1-12, 2015, <https://doi.org/10.1016/j.asej.2015.10.004>.
- [14] Y. Deng and W. Liu, "Model Predictive Load Frequency Control of Two Area Interconnected Time Delay Power System with TCSC," *2nd Asia Conference on Power and Electrical Engineering (ACPEE)*, vol. 199, pp. 1-7, 2017, <https://doi.org/10.1088/1757-899X/199/1/012064>.
- [15] E. E. Ejegi, "Model Predictive based load frequency control studies in a deregulated environment," *Ph.D. Thesis, The University of Sheffield*, 2017, <https://etheses.whiterose.ac.uk/17112/>.
- [16] H. Golpira, H. Bevrani and H. Golpira, "Application of GA Optimization for Automatic Generation Control Design in an Interconnected Power System," *Energy Conversion and Management*, vol. 52, pp. 2247–2255, 2011, <https://doi.org/10.1016/j.enconman.2011.01.010>.
- [17] H. Golpîra, H. Bevrani and H. Golpîra, "Effect of Physical Constraints on the AGC Dynamic Behaviour in an Interconnected Power System," *International Journal on Advanced Mechatronic Systems*, vol. 3, no. 2, pp. 79–87, 2011, <https://doi.org/10.1504/IJAMECHS.2011.040679>.
- [18] A. N. Gundes and L. Chow, "Controller Synthesis for Single-area and Multi-area Power Systems with Communication Delays," *American Control Conference (ACC)*, vol. 14, pp. 970-975, 2013, <https://doi.org/10.1109/ACC.2013.6579962>.
- [19] A. Gupta, Y. P. Verma and A. Chauhan, "Effect of Physical Constraints on Load Frequency Control of Deregulated Hybrid Power System Integrated with DFIG Wind Turbine," *International Journal of Engineering and Technology (IJET)*, vol. 6 no. 6, pp. 2629-2640, 2015, <https://d1wqtxtslxzle7.cloudfront.net/80382741/IJET14-06-06-182-libre.pdf>.
- [20] C. Huang, D. Yue, X. Xie and J. Xie, "Anti-Windup Load Frequency Controller Design for Multi-Area Power System with Generation Rate Constraint," *Energies*, vol. 9, pp. 1-18, 2016, <https://doi.org/10.3390/en9050330>.
- [21] S. Jian and V. Y. Hote, "PID Controller Design for Load Frequency Control: Past, Present and Future Challenges," *3rd IFAC Conference on Advances in Proportional Integral-Derivative Control, Ghent, Belgium*, vol. 2, pp. 604-609, 2018, <https://doi.org/10.1016/j.ifacol.2018.06.162>.
- [22] A. Khodabakhshian and M. Edrisi, "A New Robust PID Load Frequency Controller," *Control Engineering Practice*, vol. 16, pp. 1069–1080, 2008, <https://doi.org/10.1016/j.conengprac.2007.12.003>.
- [23] G. Kou, P. Markham, S. Hadley, T. King and Y. Liu, "Impact of Governor Dead Band on Frequency Response of the U.S. Eastern Interconnection," *IEEE Transactions on Smart Grid*, vol.12, pp. 1-10, 2015, <https://doi.org/10.1109/TSG.2015.2435258>.
- [24] S. R. Krishna, P. Singh and M. S. Das, "Control of Load Frequency of Power System by PID Controller Using PSO," *International Journal of Recent Development in Engineering and Technology*, vol. 5, no. 6, pp. 37-43, 2016, [https://www.ijrdet.com/files/Volume5Issue6/IJRDET\\_0616\\_09.pdf](https://www.ijrdet.com/files/Volume5Issue6/IJRDET_0616_09.pdf).
- [25] M. S. Kumar and S.K.V Smitha, "Design of Tuning Methods for Fractional Order PI<sup>λ</sup>D<sup>μ</sup> Controller Using PSO Algorithm," *International Journal for Research in Applied Science & Engineering Technology (IJRASET)*, vol. 2, no. XII, pp. 436-442, 2014, <http://cloud.politala.ac.id/politala/1.%20Jurusan/Teknik%20Informatika>.
- [26] S. Mirjalili, "The Ant Lion Optimization," *Advances in Engineering Software*, vol. 83, pp. 80–98, 2015, <https://doi.org/10.1016/j.advengsoft.2015.01.010>.
-

- [27] D. K. Mishra, A. Mohanty and P. Ray, "Multi-area Automatic Generation Control with FOPID and TID Controller," *International Journal of Control Theory and Application*, vol. 10, no. 6, pp. 397-410, 2017, [https://www.serialsjournals.com/abstract/69741\\_43-dillip\\_k\\_mishra.pdf](https://www.serialsjournals.com/abstract/69741_43-dillip_k_mishra.pdf).
- [28] Y. Mobarak, "Effects of the Droop Speed Governor and Automatic Generation Control AGC on Generator Load Sharing of Power System," *International Journal of Applied Power Engineering (IJAPE)*, vol. 4, no. 2, pp. 84-95, 2015, <https://doi.org/10.1109/CTPP.2014.7040611>.
- [29] J. Morsali, K. Zare and M. T. Hagh, "Appropriate Generation Rate Constraint (GRC) Modeling Method for Reheat Thermal Units to Obtain Optimal Load Frequency Controller (LFC)," *The 5th Conference on Thermal Power Plants (IPGC)*, vol. 8, pp. 29-34, 2014, <https://doi.org/10.1109/CTPP.2014.7040611>.
- [30] P. G. Naidu and R. G. Rao, "Load Frequency Control for Two-area Interconnected Power System by Using Sliding Mode Controller," *International Journal of Electrical, Electronics and Data Communication*, vol. 4, no. 10, pp. 11-18, 2016, <https://doi.org/10.1109/RTEICT42901.2018.9012156>.
- [31] M. Ozkop, I. H. Altas, and A. M. Sharaf, "Load Frequency Control in Four Area Power Systems Using Fuzzy Logic PI Controller," *16th National Power Systems Conference*, vol. 1, pp. 233-240, 2010, <https://www.iitk.ac.in/npsc/Papers/NPSC2010/5016.pdf>.
- [32] I. Pan and S. Das, "Fractional-order load-frequency control of interconnected power systems using chaotic multi-objective optimization," *Applied and Soft Computing Journal*, vol. 67, pp. 1-17, 2015, <https://doi.org/10.1016/j.asoc.2014.12.032>.
- [33] D. G. Padhan and S. Majhi, "A New Control Scheme for PID Load Frequency Controller of Single-area and Multi-area Power Systems," *ISA Transactions*, vol. 52, pp. 242-251, 2013, <https://doi.org/10.1016/j.isatra.2012.10.003>.
- [34] S. Prakash and S. K. Sinha, "Intelligent PI Control Technique in Four Area Load Frequency Control of Interconnected Hydro-thermal Power System," *2012 International Conference on Computing, Electronics and Electrical Technologies [ICCEET]*, vol. 2, pp. 145-150, 2012, <https://doi.org/10.1109/ICCEET.2012.6203749>.
- [35] R. Satheeshkumar and R. Shivakumar, "Ant Lion Optimization Approach for Load Frequency Control of Multi-Area Interconnected Power Systems," *Circuits and Systems*, vol. 7, pp. 2357-2383, 2016, <https://doi.org/10.4236/cs.2016.79206>.
- [36] H. A. Shayanfar, H. Shayeghi and A. Molaei, "Multi-Source Power System LFC Using the Fractional Order PID Controller Based on SSO Algorithm Including Redox Flow Batteries and SMES," *International Conference on Artificial Intelligence*, vol. 4, pp. 300-306, 2016, <https://www.proquest.com/openview/bdbfe2bc1e94f2be170770c3ff37e573/1?pq-origsite=gscholar&cbl=1976349>.
- [37] V. P. Singh, N. Kishor and P. Samuel, "Communication Time Delay Estimation for Load Frequency Control in Two-area Power System," *Ad Hoc Networks*, vol. 000, pp. 1-17, 2015, <https://doi.org/10.1016/j.adhoc.2015.10.010>.
- [38] T. Aleksei, E. Petlenkov & J. Belikov, "FOMCON: a MATLAB Toolbox for Fractional-order System Identification and Control," *International Journal of Microelectronics and Computer Science*, vol. 2, no. 2, pp. 51-62, 2011, <https://www.infona.pl/resource/bwmeta1.element.baztech-article-LOD7-0029-0056>.
- [39] S. Sondhi and Y. V. Hote, "Fractional Order PID Controller for Load Frequency Control," *Energy Conversion and Management*, vol. 85, pp. 343-353, 2014, <https://doi.org/10.1016/j.enconman.2014.05.091>.
- [40] B. Sonker, D. Kumar, and P. Samuel, "A Modified Two-degree of Freedom Internal Model Control Configuration for Load Frequency Control of a Single Area Power System," *Turkish Journal of Electrical Engineering & Computer Sciences*, vol. 25, pp. 4624-4635, 2017, <https://doi.org/10.3906/elk-1701-225>.
- [41] W. Tan, "Tuning of PID Load Frequency Controller for Power Systems," *International Journal Energy Conversion and Management*, vol. 50, pp. 1465-1472, 2009, <https://doi.org/10.1016/j.enconman.2009.02.024>.

- [42] W. Tan, "Unified Tuning of PID Load Frequency Controller for Power Systems via IMC," *IEEE Transactions on Power Systems*, vol. 25, no. 1, pp. 341-350, 2010, <https://doi.org/10.1109/TPWRS.2009.2036463>.
- [43] W. Tan, "Decentralized Load Frequency Controller Analysis and Tuning for Multi-area Power Systems," *Energy Conversion and Management*, vol. 52, pp. 2015–2023, 2011, <https://doi.org/10.1016/j.enconman.2010.12.011>.
- [44] W. Tan, Y. Hao and D. Li D, "Load Frequency Control in Deregulated Environments via Active Disturbance Rejection," *Electrical Power and Energy Systems*, vol. 66, pp. 166–177, 2015, <https://doi.org/10.1016/j.enconman.2010.12.011>.
- [45] W. Tan, S. Chang and R. Zhou, "Load Frequency Control of Power Systems with Non-linearities," *Institute of Engineering and Technology Generation Transmission and Distribution.*, vol. 11, pp. 4307-4313, 2017, <https://doi.org/10.1049/iet-gtd.2017.0599>.
- [46] J. M. Thangaiah, and R. Parthasarathy, "Delay-dependent Stability Analysis of Power System Considering Communication Delays," *International Transaction on Electrical Energy System*, vol. 20, pp. 1–13, 2016, <https://doi.org/10.1002/etep.2260>.
- [47] A. Zamani, S. M. Barakati and S. Yousofi-Darmain, "Design of a Fractional Order PID Controller Using GBMO Algorithm for Load–Frequency Control with Governor Saturation Consideration," *ISA Transactions*, vol. 45, pp. 1–11, 2016, <https://doi.org/10.1016/j.isatra.2016.04.021>.